Electronic Supplementary Information

Electrocatalyst-induced kinetic modulation of anion-based redox mediators in aqueous iron-chromium redox flow batteries

Vithiya Muralidharan,‡ Ryeong-ah Kim,‡ Ji-Eun Jang, and Hyun-Wook Lee*

School of Energy and Chemical Engineering, Ulsan National Institute of Science and Technology (UNIST), Ulsan 44919, Republic of Korea.

*Email: hyunwooklee@unist.ac.kr

‡ These authors have contributed equally.

Experimental Procedures

Synthesis Procedure

Preparation of potassium hexacyanochromate ($K_3[Cr(CN)_6]$) The $K_3[Cr(CN)_6]$ compound was synthesized by adapting previously reported protocols. Initially, chromium(III) acetate hydrate ($Cr(C_2H_3O_2)_3.H_2O$, 5 g; JUNSEI, Cr 21-25%) was dissolved in 20 mL of distilled water (DI water) under ambient conditions to produce a deep green solution. In parallel, potassium cyanide (KCN, 8.93 g; Alfa Aesar, 96.0%) was dissolved in 30 mL of DI water and brought to a vigorous boil under continuous stirring. With active stirring (300 rpm), the $Cr(C_2H_3O_2)_3.H_2O$ solution was added slowly to the boiling KCN solution. Immediately following the addition, activated charcoal (0.24 g; Supelco) was introduced as a reaction facilitator. The reaction mixture was maintained to boil with constant agitation for 5 min to ensure complete complexation. The hot suspension was filtered under reduced pressure to remove the activated charcoal, yielding a clear bright red filtrate. The solution was partially concentrated by evaporation and subsequently cooled gradually to room temperature, exploiting the inverse solubility profile of $K_3[Cr(CN)_6]$ to induce crystallization. The resulting crystalline product was isolated by vacuum filtration and washed with methanol and ethanol followed by drying at 40°C in vacuum to obtain pale yellow product.

Electrodeposition of metal on separable glassy carbon electrode (SGCE) Bismuth (Bi), tin (Sn) and indium as anti-catalysts were decorated on GCE by electrodeposition. For each metal, a 20 ml deposition solution was prepared by dissolving 10 mM of the corresponding metal chloride, Bismuth (III) chloride ($BiCl_3$; Alfa Aesar, 99.9%), Tin (II) chloride ($SnCl_2$; Alfa Aesar , 98.0%), Indium (II) chloride ($InCl_3$; Sigma Aldrich 98.0%) in 1 M hydrochloric acid (HCl), which served as a constant supporting electrolyte across all the experiments. The counter (CE) and the reference electrode (RE) were platinum (Pt) wire and Ag/AgCl electrode (3 M KCl), respectively. Two different 3 mm GCEs were employed as the working electrode (WE), with the integrated GCE for electrochemical half-cell analysis and separable type for optical microscopy (OM). Prior to electrodeposition, each GCE was polished sequentially with 1.0, 0.3, 0.05 µm alumina suspensions (Al_2O_3) on both nylon and microcloth pads and then sonicated in ethanol for 15 minutes to ensure a clean electrode surface free from residual contaminants. Electrodeposition was conducted in potentiostatic mode using chronoamperometry with an EC-lab potentiostat (BioLogic), with deposition times varied systematically as needed for each metal. The applied potentials specific to each metal chloride precursor are detailed in **Table S1.**

Electrodeposition of anti-catalyst on graphite felt (GF) Graphite felt electrodes of dimension 5 cm^2 (2.0 cm × 2.5 cm) (XF-30a, TOYOBO) was heat treated at 500 ^oC for 5 h in ambient atmosphere which increases their surface wettability. The thermally treated graphite felt (TGF) were rinsed with distilled water and dried at 40 ^oC for 24 h prior to electrodeposition process. Bismuth was deposited onto TGF from a 0.2 M bismuth deposition solution, prepared by dissolving $BiCl_3$ (Alfa Aesar, 99.9%) in 2.5 M HCl. Deposition was conducted for under two different durations of 5 and 10 minutes with an interval of 20 s for each duration, aimed at achieving more uniform and controlled bismuth deposition.

Electrochemical characterization

Cyclic voltammetry (CV) CV measurements were performed using a conventional three-electrode setup consisting of Hg/HgO as the RE (1 M KOH), a platinum wire as the CE, and a 3 mm integrated GCE as WE. Prior to all electrochemical characterization, the WE were polished to a mirror finish through sequential mechanical polishing with alumina suspensions of 1.0, 0.3, 0.05 µm particle sizes, followed by ultrasonic cleaning in ethanol for 15 minutes to remove residual contaminants. CV tests were conducted in 0.1 M synthesized $K_3[Cr(CN)_6]$ dissolved in 1 M NaCN (Alfa Aesar, 95% min) solution. For comparison to the posolyte side, the CV was performed in a solution containing 0.05 M $K_4[Fe(CN)_6]$ (Sigma Aldrich, 98.5 - 102.0%) dissolved in 1 M NaCl (Alfa Aesar, 99.0%). The CVs were performed with ohmic drop correction using the ZIR compensation function in EC-Lab (BioLogic), applying 85 % compensation of sthe solution resistance.

Linear Sweep Voltammetry (LSV) LSV analyses were conducted using the same three-electrode system described above. The measurements were carried out in 1 M NaCN solution without active material to assess the baseline electrochemical response of the system.

Electrochemical Impedance Spectroscopy (EIS) EIS were conducted under potentiostatic control at -1.1 V vs SHE using a sinusoidal AC perturbation of 30 mV amplitude. The frequency range spanned from 3 MHz to 100 mHz. All EIS measurements were performed in 0.1 M synthesized $K_3[Cr(CN)_6]$ dissolved in 1 M NaCN. Prior to all electrochemical analyses, the electrolyte solutions were purges with nitrogen gas (N_2) for 10 minutes to remove dissolved oxygen and maintain an inert atmosphere.

Stability test The stability test has been carried out for two half cells. One comprising of 0.1 M $K_3[Cr(CN)_6]$ in 2 M NaCN and the other with 0.1 M $CrCl_3$ in 1 M HCl. The working electrode was the Bi deposited SGCE, a Hg/HgO reference electrode filled with 1 M KOH and a Pt plate (1 cm × 1 cm) served as the reference and counter electrode, respectively.

Full cell test The full cell test was performed with a posolyte containing 40 mL of 0.4 M $K_4[Fe(CN)_6].3H_2O$ (Sigma-Aldrich, 98.5%) with 2.5 M NaCl (Sigma-Aldrich, ≥ 99.5%) as supporting electrolyte and a negolyte containing 30 mL of 0.4 M $K_3[Cr(CN)_6]$ (as-synthesized) with 2.0 M NaCN (Sigma-Aldrich, 97%) and 0.5 M NaOH (Sigma-Aldrich, 98%) as the supporting electrolyte. The flow cell assembly (TS CHEM) comprises of the bismuth deposited TGF of dimension 5 cm^2 (2.0 cm × 2.5 cm), bipolar plate, copper current collector, and Nafion membrane (NRE-212, Nafion perfluorinated membrane, Sigma-Aldrich, 0.002 inch thick) was soaked in 0.1 M HCl for 30 min and rinsed in DI water. The Bi-TGF in a stack cell were compressed ~70%. The electrolyte circulation was facilitated by pump drives (JenieWell, JWSE600) using Norprene tubing (Masterflex Norprene, 3.175 mm thickness, O.D. 6.35 mm and I.D. 3.18 mm). The flow rate was maintained at ~40 mL min^{-1} (50 rpm) throughout the experiment. The components of the full cell were assembled in a commercial flow battery framework. Prior to cycling, the system was optimized by circulating the electrolyte through the electrode for 1 hour without external current to ensure complete wettability of the electrode. Galvanostatic charge-discharge experiments were carried out using an EC-Lab Potentiostat (BioLogic) under ambient conditions. The charging and discharging cycles were performed at a constant current of 500 mA (± 100 mA cm^{-2}) with the voltage range of 1.0 to 1.9 V rather than the explicit SOC control. The effective SOC window accessed during the cycle was therefore evaluated from the discharge capacity relative to the theoretical capacity of the negolyte. For a 0.4 M negolyte, the theoretical capacity is 10.72 Ah L^{-1}. The cell delivered a stable initial discharge capacity of 9.81 Ah L^{-1}, corresponding to a capacity utilization of approximately 91.5 %. As the lower cut-off voltage corresponds to the fully discharged state, this analysis indicates that the full cell was cycled across an effective operational SOC range of approximately 0 % to 91.5 %.

Material Characterization

Scanning Electron Microscopy (SEM) SEM analysis was conducted to characterize the morphology of bismuth electrodeposited on graphite felt samples. Imaging was performed with an accelerating voltage of 5kV. The samples were dried in vacuum oven at 40^o for 24 h before imaging. Samples were mounted on conductive tape and observed under vacuum conditions. Magnifications from ×1.00k to ×5.00k were used to investigate the distributed of deposited bismuth. Elemental mapping was conducted to visualize the distribution and localization of key elements within the electrodeposited felt as shown in Figure S9.

Ultraviolet Visible Spectroscopy (UV-Vis) The dissolution of bismuth in the electrolyte was investigated using UV-Vis spectroscopy. For this investigation, 5 mL of electrolyte after the stability test were drawn out and diluted with 1.0 NaCN to 0.001 M (1/100 times dilution).[1] Bismuth nitrate solution was used as the control standard for comparison.

Optical Microscopy (OM) The surface morphology of the separable glassy carbon electrode was examined using an optical microscope (OLYMPUS BX53M) equipped with a digital imaging system (Techsan Co. Ltd, Tech Xcam III camera). Following electrodeposition at varying durations, the electrode was thoroughly rinsed with 25% ammonia solution (Emsure) to remove residual electrolyte. Subsequently, the electrode was dried in a box furnace at 60°C to ensure complete removal of moisture and contaminants prior to imaging.

Measurement of kinetic parameters

Diffusion coefficient (D_O and D_R) The diffusion coefficient was obtained using Randles-Sevick equation for reversible system. It was adaptable because (1) linear relationship was observed between peak current and square root of scan rate and (2) peak potential difference was less than 300 mV which was relevant to quasi-reversible region. The equation uses the relationship between the cathodic peak current density, $i_{p,c}$, and the diffusion coefficient, D_o, since the half-cell was prepared by dissolving the synthesized $K_3[Cr(CN)_6]$ without $K_4[Cr(CN)_6]$. But for the $[Fe(CN)_6]^{4-/3-}$, since the electrolyte contained identical quantities of $[Fe(CN)_6]^{3-}$ and $[Fe(CN)_6]^{4-}$, $i_{p.c}$ and $i_{p,a}$ were estimated respectively.

$$i_{p,c} = (2.69 \times 10^5) \cdot n^{\frac{3}{2}} \cdot D_O^{\frac{1}{2}} \cdot C_O^* \cdot v^{\frac{1}{2}} \tag{1}$$

$$i_{p,a} = (2.69 \times 10^5) \cdot n^{\frac{3}{2}} \cdot D_R^{\frac{1}{2}} \cdot C_R^* \cdot v^{\frac{1}{2}} \tag{2}$$

$i_{p,c}$	Cathodic peak current density (A cm^{-2})
$i_{p,a}$	Anodic peak current density (A cm^{-2})
n	Number of electrons transferred for the redox reaction
D_O	Diffusion coefficient of oxidative species (cm^2 s^{-1})
D_R	Diffusion coefficient of reductive species (cm^2 s^{-1})
C_O^*	Bulk concentration of oxidative species (mol cm^{-3})
C_R^*	Bulk concentration of reductive species (mol cm^{-3})
v	Scan rate (V s^{-1})

Where the oxidative species is reduced to reductive species by accepting one electron ($n = 1$). The CV was conducted with various scan rates (20, 40, 60, 80, 100, 150, and 200 mV s^{-1}).

Standard Rate Constant (k_0) For the $[Cr(CN)_6]^{3-}$, where the solution comprised predominantly the oxidative species, the charge transfer coefficient (α) was assumed to be 0.5. Given that the solution contained only $[Cr(CN)_6]^{3-}$ and considering the nearly identical molar masses of the oxidized and reduced forms, the k_0 was calculated using the following simplified form:

$$k_0 = (\pi \cdot D_O \cdot f \cdot v)^{1/2} \cdot \Psi \tag{3}$$

Whereas in the case of $[Fe(CN)_6]^{4-/3-}$, which contained equal concentrations of both oxidative and reductive species, the diffusion coefficients for each species were individually calculated.[2] Therefore, the k_0 was calculated with using equation (4) without any simplification.

$$k_0 = \left[\frac{(\pi \cdot D_O \cdot f \cdot v)^{1/2}}{(D_O/D_R)^{\alpha/2}}\right] \cdot \Psi \tag{4}$$

k_0	Standard rate constant (cm s^{-1})
D_O	Diffusion coefficient of oxidative species (cm^2 s^{-1})
D_R	Diffusion coefficient of reductive species (cm^2 s^{-1})
f	$f = (n \cdot F) / (R \cdot T)$
	n is the number of electrons transferred for the redox reaction
	F is the Faraday constant (96485 C mol^{-1})
	R is the ideal gas constant (8.314 J mol^{-1} K^{-1})

T is the absolute temperature in K (T = 298.15 K)

v Scan rate (V s^{-1})

α Charge transfer resistance ($0 < \alpha < 1$)

Ψ Nicholson number

Ψ is the Nicholson number that is related to peak potential difference (ΔE_p) which was measured from the CV curves. The Ψ values has been obtained from Nicholson's classic paper.[3, 4]

$$\Psi = \frac{(-0.6228 + 0.0021\,\Delta E_p)}{(1 - 0.017\,\Delta E_p)} \qquad (5)$$

Herein the Nicholson dimensionless number is calculated by substituting the peak potential separation in equation (5). **Table S3** covers the reversible rang up to 200 mV, but in our study the active species undergoes a quasi-reversible redox reaction. Therefore, Klinger and Kochi method for an irreversible reaction was combined with the Nicholson method.[5]

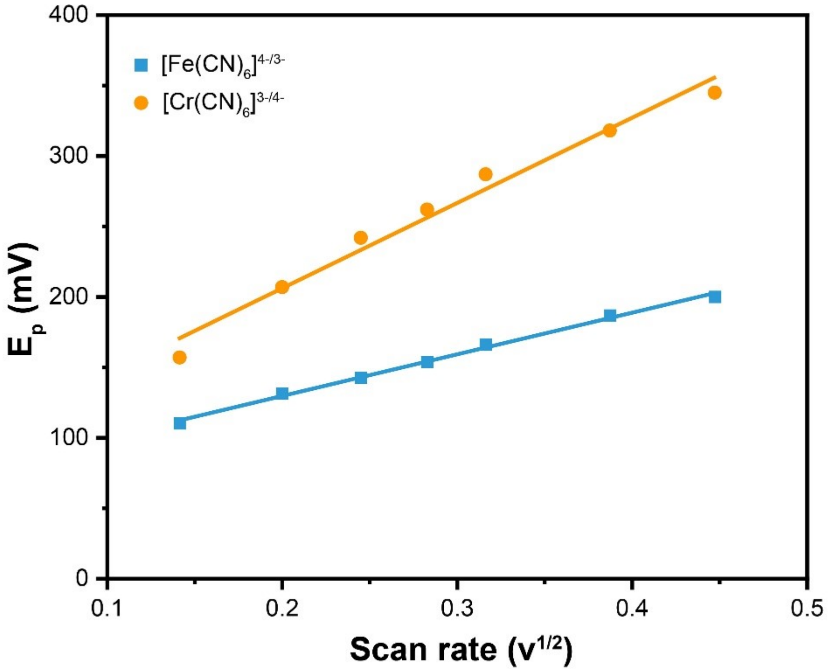

Figure S1. Peak potential separation linearly fitted as a function of square root of scan rate corresponding to $[Fe(CN)_6]^{4-/3-}$ and $[Cr(CN)_6]^{3-/4-}$ for the CV measured in $[Fe(CN)_6]^{4-/3-}$ at various scan rates from 20 to 200 mV s^{-1} measured in 0.05 M $K_3[Fe(CN)_6]$ and 0.05 M $K_4[Fe(CN)_6]$ with 1 M NaCl as supporting electrolyte and $Cr(CN)_6]^{3-/4-}$ at various scan rates from 20 to 200 mV s^{-1} measured in 0.1 M $K_3[Cr(CN)_6]$ with 1M NaCN as supporting electrolyte, respectively.

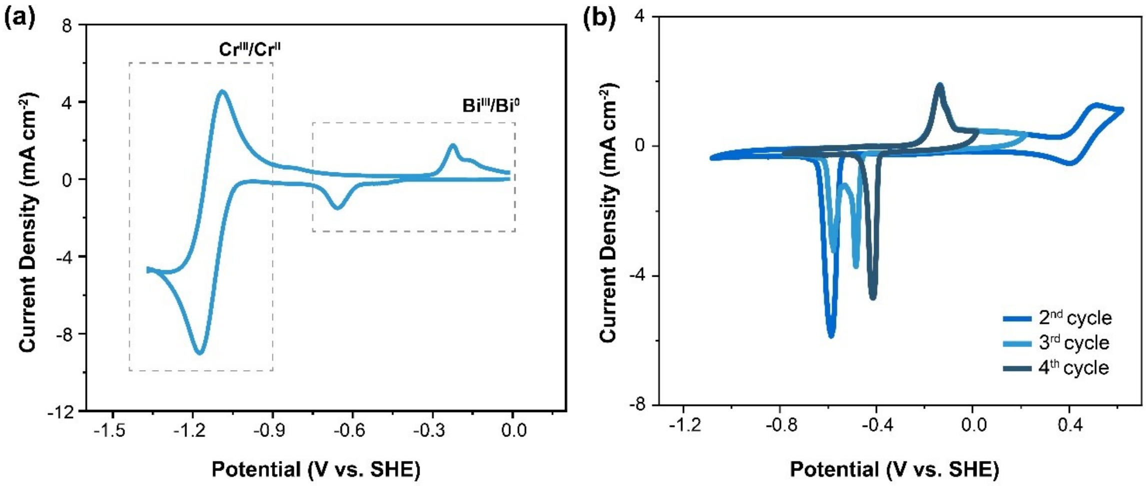

Figure S2. (a) CV of $[Cr(CN)_6]^{4-/3-}$ and $Bi^{III/0}$ with the SGCE modified with bismuth at a scan rate of 20 mV s^{-1}. The left redox peaks correspond to the redox reaction between Cr^{III} and Cr^{II}; the right redox peaks refer to the redox reaction between Bi^{III} and Bi^0 **(b)** Repeated deposition/dissolution of CV curves of bismuth redox reaction, demonstrating evolution of peak positions and current density at a scan rate of 20 mV s^{-1}.

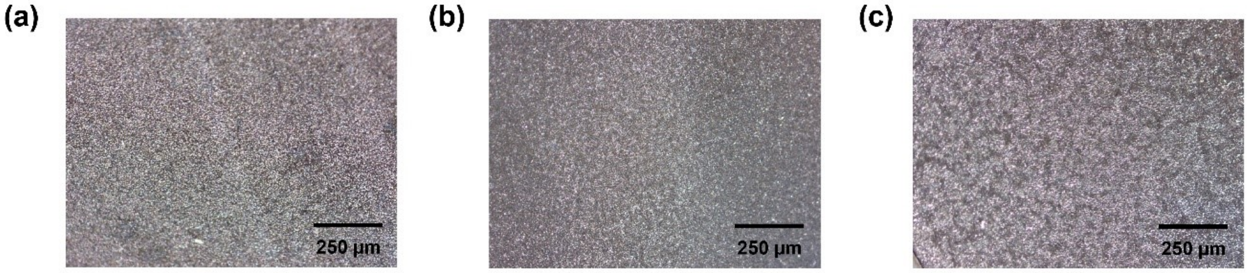

Figure S3. OM images of SGCE surface after bismuth deposition at **(a)** 30 s, **(b)** 40 s, and **(c)** 60 s.

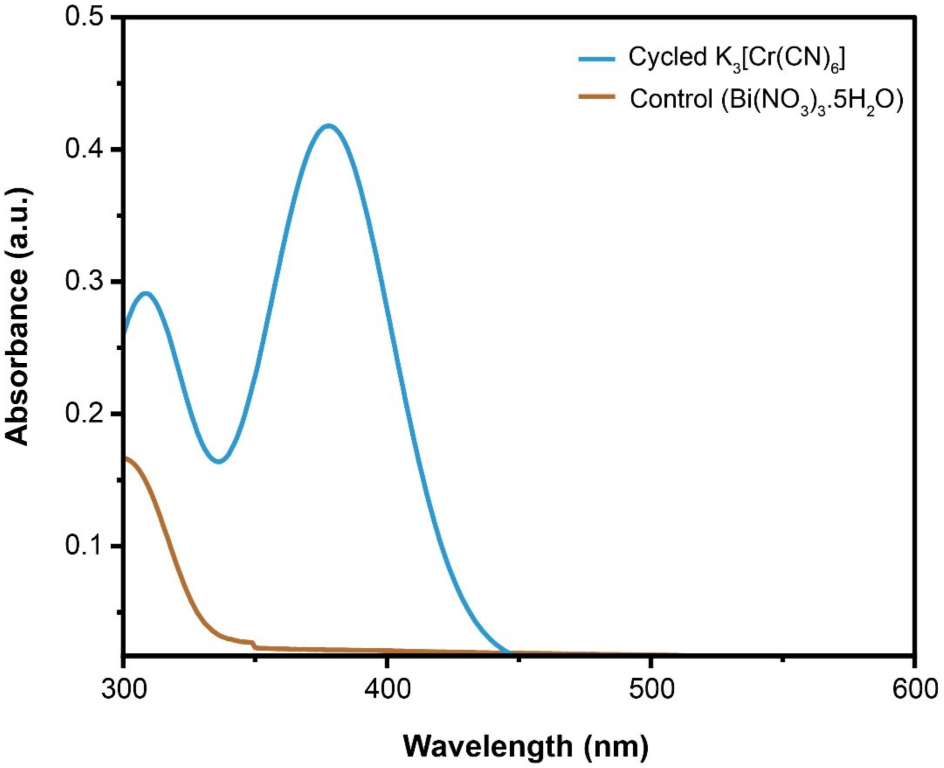

Figure S4. UV-vis spectrum of the $K_3[Cr(CN)_6]$ (blue) after the stability test compared with the bismuth nitrate (brown) spectrum demonstrating that there is no dissolution of bismuth into the electrolyte.

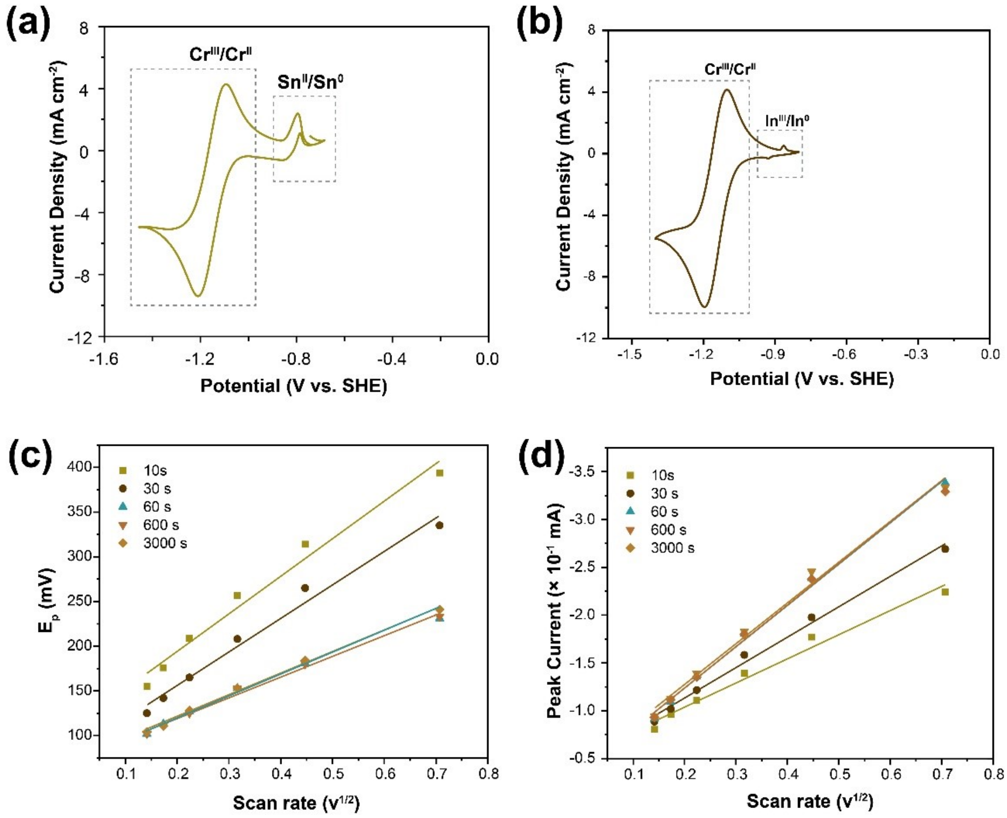

Figure S5. (a) CV of $[Cr(CN)_6]^{4-/3-}$ and $Sn^{II/0}$ with the SGCE modified with tin at a scan rate of 20 mV s^{-1}. The left redox peaks correspond to the redox reaction between Cr^{III} and Cr^{II}; the right redox peaks refer to the redox reaction between Sn^{II} and Sn^{0}. **(b)** CV of $[Cr(CN)_6]^{4-/3-}$ and $In^{III/0}$ with the SGCE modified with indium at a scan rate of 20 mV s^{-1}. The left redox peaks correspond to the redox reaction between Cr^{III} and Cr^{II}; the right redox peaks refer to the redox reaction between In^{III} and In^{0} **(c)** Peak potential separation and **(d)** Peak current linearly fitted against the square root of scan rate with Sn deposited SGCE at different deposition durations (10, 30, 60, 600, and 3,000 s).

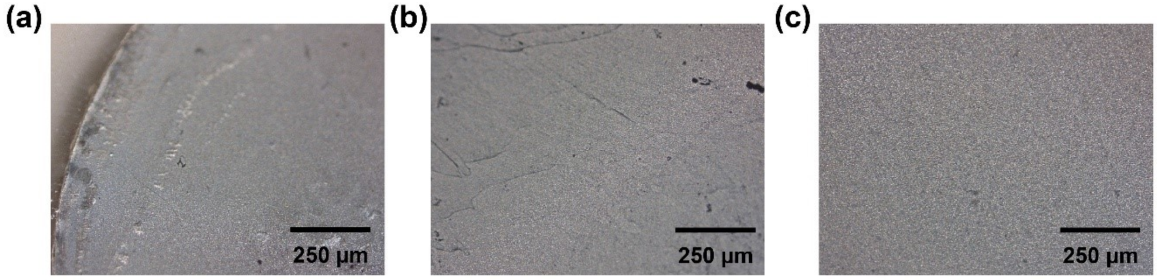

Figure S6. OM images of SGCE surface after tin deposition at **(a)** 30 s, **(b)** 60 s, and **(c)** 90 s.

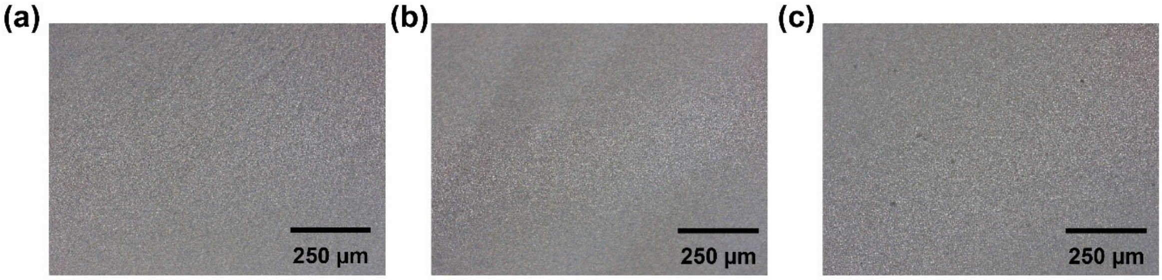

Figure S7. OM images of SGCE surface after indium deposition at **(a)** 30 s, **(b)** 60 s, and **(c)** 90 s.

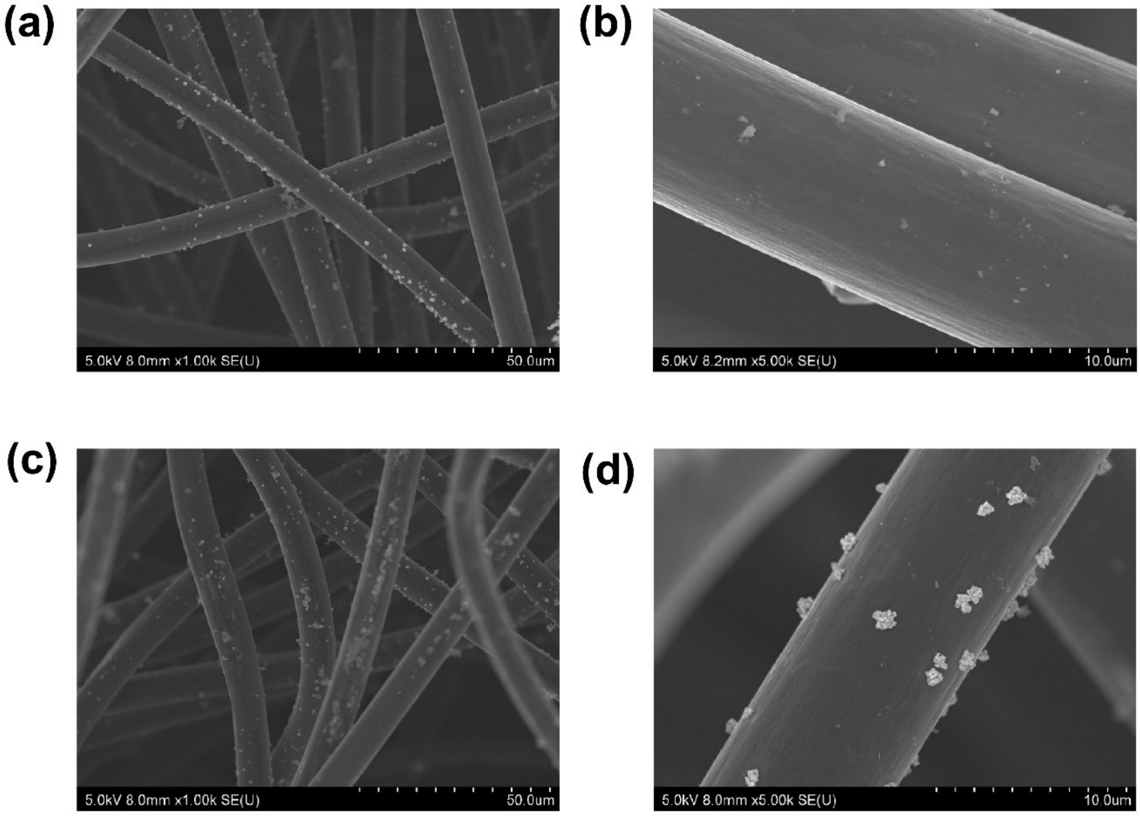

Figure S8 SEM images of bismuth electrodeposited on carbon felt. **(a,b)** Morphology after 2.5 min deposition pulsed 2 times with 20 sec of rest, shows uniform deposition of Bi along the graphite felt. **(c,d)** Morphology after 5 min deposition pulsed 2 times with 20 sec of rest, shows a larger aggregated bismuth deposition.

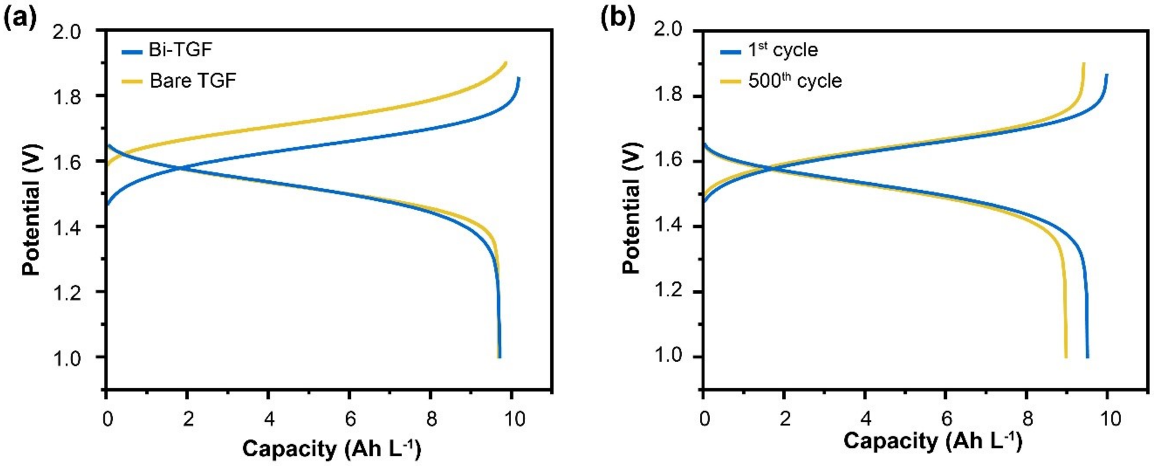

Figure S9 Galvanostatic charge-discharge voltage profiles for the full cell (a) Voltage profiles of Bi-TGF and bare TGF electrodes at current density of 100 mA cm^{-2}, illustrating lower overpotential for the Bi-TGF (b) Comparison of the 1st and 500th cycle for the Bi-TGF electrode, indicating minimal polarization growth and stable cycling behavior.

As shown in Figure S9b, the voltage-capacity profiles recorded at the 1st and 500th cycles for the Bi-TGF electrode are compared to evaluate the evolution of polarization during extended cycling. The close overlap of both the charge and discharge plateaus, together with the absence of significant growth in voltage hysteresis, indicates minimal increase in polarization and negligible degradation of interfacial reaction kinetics over prolonged operation. These sdemonstrate that the kinetic enhancement imparted by the Bi-TGF electrode is preserved throughout the extended cycling without alteration in the reaction pathway.

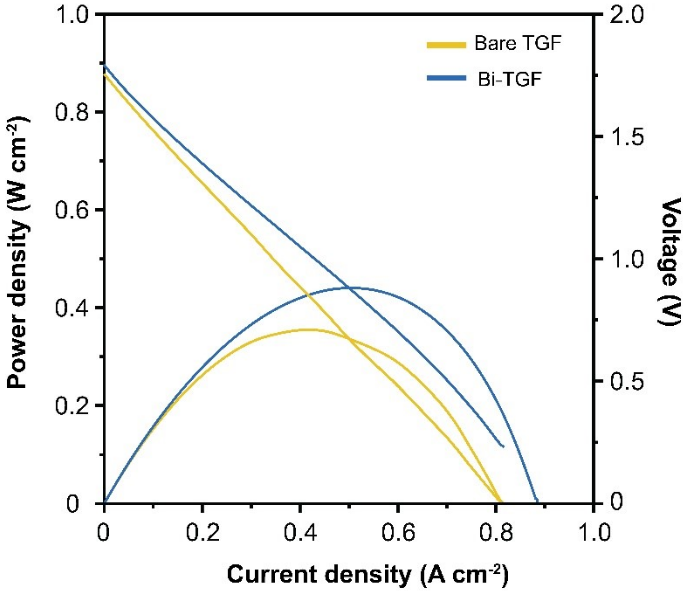

Figure S10. Polarization curves and power density as a function of current densities of full cell employing bare TGF and Bi-TGF electrode measured under identical conditions.

s

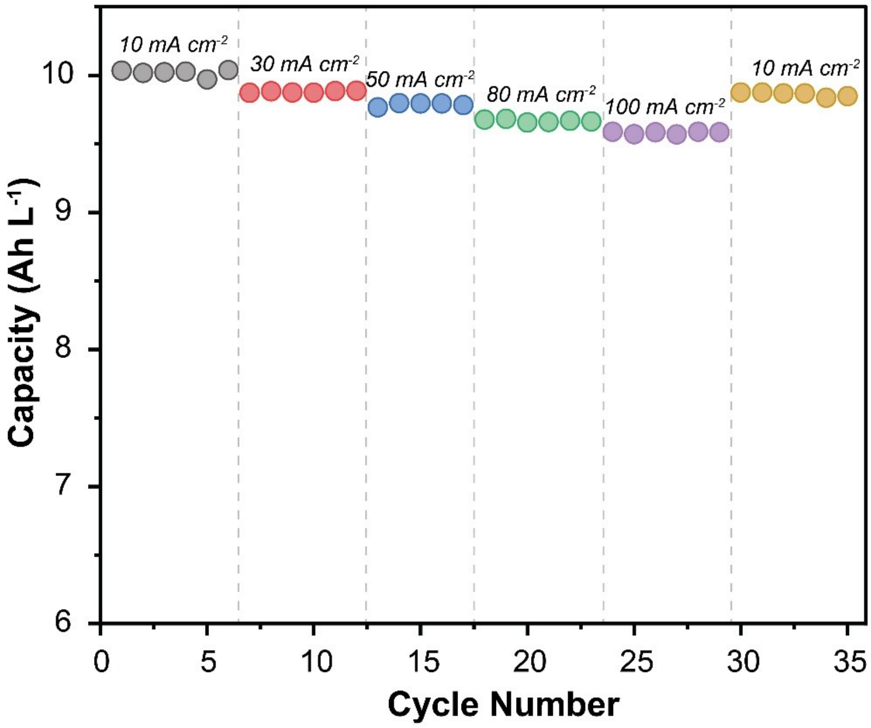

Figure S11. Rate capability performance of the full cell evaluated under stepwise varying current densities. The discharge capacity is plotted as a function of cycle number, and the applied current density is sequentially increased from 10 mA cm^{-2} to 100 mA cm^{-2}. The grey dashed lines indicate the transitions between different current densities.

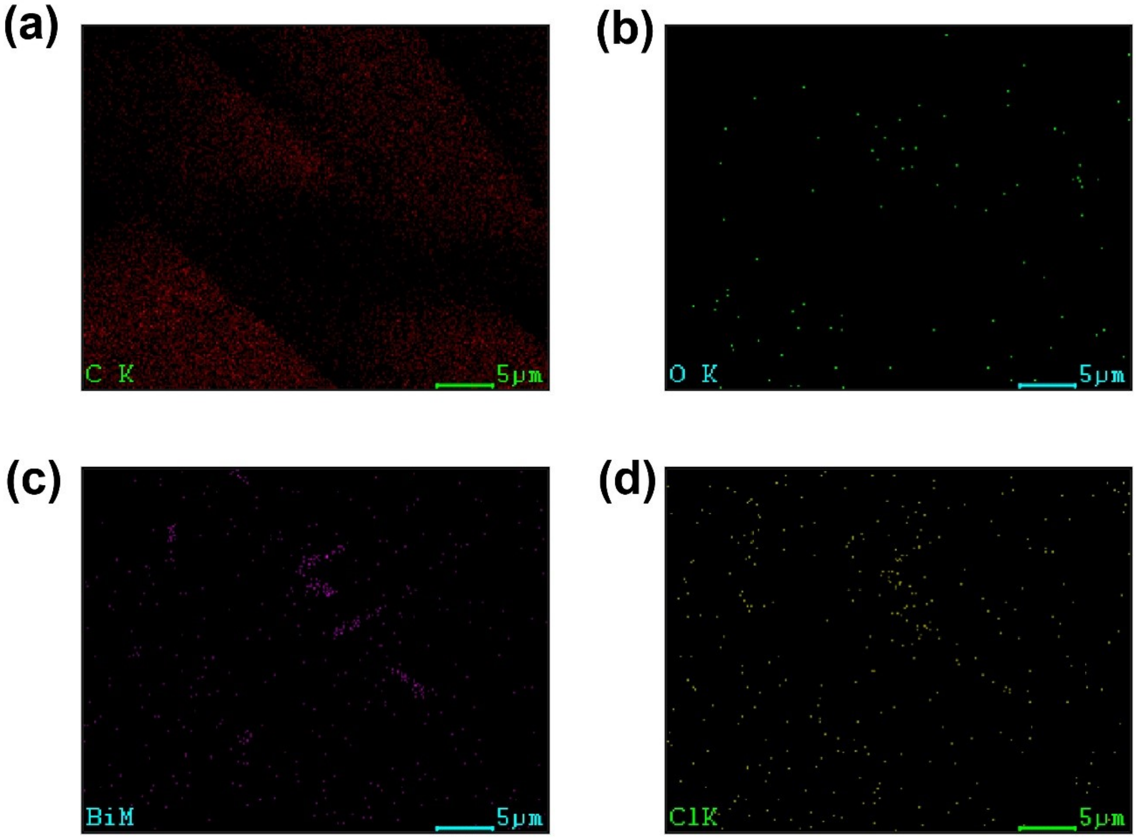

Figure S12. Elemental mapping images of the bismuth deposited graphite felt **(a)** carbon **(b)** oxygen **(c)** bismuth **(d)** chlorine (The compositions were provided in Table S4).

Table S1. Electrodeposition solution composition and applied potential for metal electrodeposition

	Active material (10 mM)	Supporting material (1 M)	Applied potential (V vs SHE)
Bi	$BiCl_3$	HCl	-0.3
Sn	$SnCl_2$	HCl	-0.65
In	$InCl_3$	HCl	-0.9

Table S2. The relationship between Ψ and ΔE_p obtained by Nicholson's method

Ψ (dimensionless)	ΔE_p
20	61
7	63
6	64
5	65
4	66
3	68
2	72
1	84
0.75	92
0.5	105
0.35	121
0.25	141
0.1	212

Table S3. Slope and intercept for the evaluated metal deposited SGCE

	i_{pa}/i_{pc}	**Slope**	**Intercept**	**R^2**
$K_3[Fe(CN)_6]$ (bare)	i_{pa}	2.131	0.173	0.987
	i_{pc}	-2.993	-0.115	0.998
$K_3[Cr(CN)_6]$ (bare)	i_{pa}	0.013	0.005	0.970
	i_{pc}	-0.033	-0.003	0.998
$K_3[Cr(CN)_6]$ (Bi@SGCE)	i_{pa}	0.153	-0.003	0.994
	i_{pc}	-0.196	0.009	0.999
$K_3[Cr(CN)_6]$ (Sn@SGCE)	i_{pa}	0.037	0.004	0.985
	i_{pc}	-0.047	-0.004	0.998
$K_3[Cr(CN)_6]$ (In@SGCE)	i_{pa}	0.029	0.005	0.945
	i_{pc}	-0.037	-0.005	0.990

Deposition time	R_s (Ω)	R_{ct} (Ω)	Q (F s^{n-1})	n	W (Ω $s^{-1/2}$)
0 s	20.84	144.53	2.37×10^{-5}	0.85	62.4
30 s	14.90	39.08	9.64×10^{-4}	0.81	78.9
40s	14.99	49.60	1.43×10^{-3}	0.73	109.6

Table S4. Electrochemical Impedance Spectroscopy fitting parameters

Table S5. Elemental mapping results of the Bi-TGF

Element	Mass Norm (%)	Atom (%)
C	93.09	99.05
Bi	5.78	0.35
Cl	0.70	0.25
O	0.43	0.35
	100.0	100.0

Table S6. Comparison of key electrochemical performance metrics for ICRFBs reported in literature and present work

Modified Electrode	Current density	Coulombic efficiency (CE)	Voltage efficiency (VE)	Energy efficiency (EE)	Cycle life	References
Bi-TGF	**100 mA cm^{-2}**	**99.29 %**	**75.82 %**	**75.22 %**	**500 cycles**	**This work**
PBi/TCF (Gradient Bi-C electrode)	120 mA cm^{-2}	~98 %	-	81.36 %	500 cycles (Refreshed electrolyte)	[6]
TBCC (Bi modified carbon cloth)	140 mA cm^{-2}	~ 98%	-	82.9 %	200 cycles	[7]
Bi/N-GF (Bismuth coated B-doped graphite felt)	60 mA cm^{-2}	97.7 %	-	85.8 %	100 cycles	[8]
AgBi-TGF (Silver bismuth bimetallic modified TGF)	60 mA cm^{-2}	96.80 %	70.73 %	68.74 %	80 cycles	[9]

REFERENCES

1. L. Jeftic and S. W. Feldberg, *J. Phys. Chem.*, 1971, **75**, 2381–2387.
2. K. Gong, Q. R. Fang, S. Gu, S. F. Y. Li and Y. S. Yan, *Energy Environ. Sci.*, 2015, **8**, 3515–3530.
3. R. S. Nicholson and I. Shain, *Anal. Chem.*, 1964, **36**, 706–723.
4. R. S. Nicholson, *Anal. Chem.*, 1965, **37**, 1351–1355.
5. I. Lavagnini, R. Antiochia and F. Magno, *Electroanal.*, 2004, **16**, 505–506.
6. M. Wu, S. M. Liu, H. F. Yuan, Z. C. Zhao, L. Qiao and X. K. Ma, *Adv. Mater.*, 2025, **37**.
7. Y. Liu, C. Guo, G. Wu, W. Lv, R. Zhou, W. Qiu, Y. Zhou, Q. Xu, C. Xu and Y. Niu, *Nano Research Energy*, 2025, **4**, e9120135.
8. H. X. Che, Y. F. Gao, J. H. Yang, S. Hong, L. D. Hao, L. Xu, S. Taimoor, A. W. Robertson and Z. Y. Sun, *New Carbon Mater.*, 2024, **39**.
9. R. Z. Li, Y. Guo, H. Yan, S. L. Yuan and M. Lin, *Chem. Commun.*, 2025, **61**, 9302–9305.